

Generating anatomical models of the heart and the aorta from medical images for personalized physiological simulations

J. Weese · A. Groth · H. Nickisch · H. Barschdorf · F. M. Weber · J. Velut · M. Castro · C. Toumoulin · J. L. Coatrieux · M. De Craene · G. Piella · C. Tobón-Gomez · A. F. Frangi · D. C. Barber · I. Valverde · Y. Shi · C. Staicu · A. Brown · P. Beerbaum · D. R. Hose

Received: 21 June 2012 / Accepted: 22 December 2012 / Published online: 30 January 2013
© International Federation for Medical and Biological Engineering 2013

Abstract The anatomy and motion of the heart and the aorta are essential for patient-specific simulations of cardiac electrophysiology, wall mechanics and hemodynamics. Within the European integrated project euHeart, algorithms have been developed that allow to efficiently generate patient-specific anatomical models from medical images from multiple imaging modalities. These models, for instance, account for myocardial deformation, cardiac wall motion, and patient-specific tissue information like myocardial scar location. Furthermore, integration of algorithms for anatomy extraction and physiological simulations has been brought forward. Physiological simulations are linked closer to anatomical models by encoding tissue properties, like the muscle fibers, into segmentation

meshes. Biophysical constraints are also utilized in combination with image analysis to assess tissue properties. Both examples show directions of how physiological simulations could provide new challenges and stimuli for image analysis research in the future.

Keywords Physiological simulation · Patient-specific anatomical model · Heart and aorta segmentation · Coronary veins · Heart motion · Wall mechanics · Pressure wave · Tissue properties

1 Introduction

Physiological simulations have specific requirements regarding personalized anatomical models. These models must represent a variety of anatomical structures and functional information. For simulating the electrophysiology in cardiac resynchronization therapy (CRT) it is, for instance, desirable to have a model comprising the anatomy including part of the coronary veins, tissue motion and scar tissue distribution in the left ventricle (see e.g., [1, 46]). In addition, physiological simulations can have specific requirements for heart structures. The wall should, for instance, be represented by the epi- and endocardial borders to allow for a transmural signal propagation in the left atrium [16].

Apart from anatomical structures, tissue properties are important for physiological simulations. Information such as muscle fiber direction in the myocardium can hardly be obtained from clinical images. Given the patient's heart anatomy, this information may be reconstructed by rule-based approaches [30, 51] or by mapping a specific atlas [43] to the patient's heart anatomy. Tissue properties can also be linked to image analysis methods. They have, for

J. Weese (✉) · A. Groth · H. Nickisch · H. Barschdorf · F. M. Weber
Philips Research Laboratories, Hamburg, Germany
e-mail: juergen.weese@philips.com

J. Velut · M. Castro · C. Toumoulin · J. L. Coatrieux
Laboratoire Traitement du Signal et de l'Image,
Université de Rennes and Unit INSERM U1099, Rennes, France

M. De Craene · G. Piella · C. Tobón-Gomez · A. F. Frangi
CISTIB, Universitat Pompeu Fabra, Barcelona, Spain

A. F. Frangi
Department of Mechanical Engineering,
The University of Sheffield, Sheffield, UK

D. C. Barber · Y. Shi · C. Staicu · A. Brown · D. R. Hose
Group of Medical Physics, School of Medicine and Biomedical
Sciences, The Royal Hallamshire Hospital,
The University of Sheffield, Sheffield, UK

I. Valverde · P. Beerbaum
Division of Imaging Sciences and Biomedical Engineering,
King's College London, London, UK

instance, been used in image registration to tailor the properties of the deformation field [23, 27, 59] for a specific application. Vice versa, a physical constraint may be used in an image analysis algorithm to estimate a tissue's material parameter.

This paper gives an overview over the image analysis methods developed in the euHeart project [22]. Section 2 summarizes the methods that have been developed to extract the heart anatomy (Sect. 2.1), vasculature (Sect. 2.2) and deformation (Sect. 2.3) from images. Section 3 describes two approaches for a closer integration of image analysis and physiological simulations. The first one integrates information for simulations in a generic anatomical model used in model-based segmentation (Sect. 3.1). The second approach uses the one-dimensional pressure equation to enforce a consistent time-series segmentation of the aorta, while measuring the speed of the pressure wave at the same time (Sect. 3.2). Section 4 illustrates use of the methods for two examples. A comprehensive heart model is generated by integrating anatomy, vasculature and deformation information (Sect. 4.1). Furthermore, the methods are used to set up and perform electrical signal propagation in the left atrium (Sect. 4.2). The paper concludes with a discussion of the results and an outlook.

2 Comprehensive anatomical models

2.1 Model-based heart segmentation

The basis for the creation of comprehensive physiological heart models are suitable patient-specific anatomical models. However, current anatomical models obtained by model-based segmentation [18, 19, 35, 42, 61] lack certain anatomical structures which are essential for physiological simulations. For example, the myocardium is currently modeled by a single layer surface in most parts of the heart. This does not allow for modeling the dimension of the myocardium, and, hence, for a transmural signal propagation [16, 49]. Therefore, in the euHeart project, double-walled structures for the left and right atrium with a volumetric mesh between endo- and epicardium [39] and a volumetric mesh for the left ventricular (LV) myocardium were introduced [33] (Fig. 1).

Anatomical models with a patient-specific myocardium thickness allow additionally for integrating myocardial viability information into the model. This is essential for electrophysiological simulations targeted to treatments like CRT. Figure 2 illustrates the processing pipeline exemplarily for the scar distribution in the LV myocardium (Fig. 2, [33]). An anatomical reference model including the LV epi- and endocardium is adapted to 3D images like

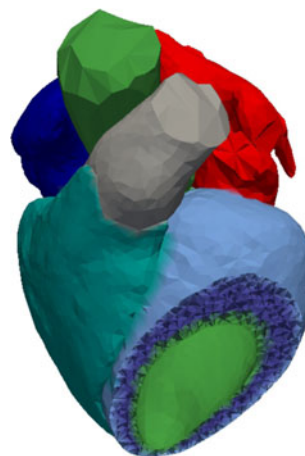


Fig. 1 Heart model used for model-based segmentation with a volumetric mesh for the left ventricle

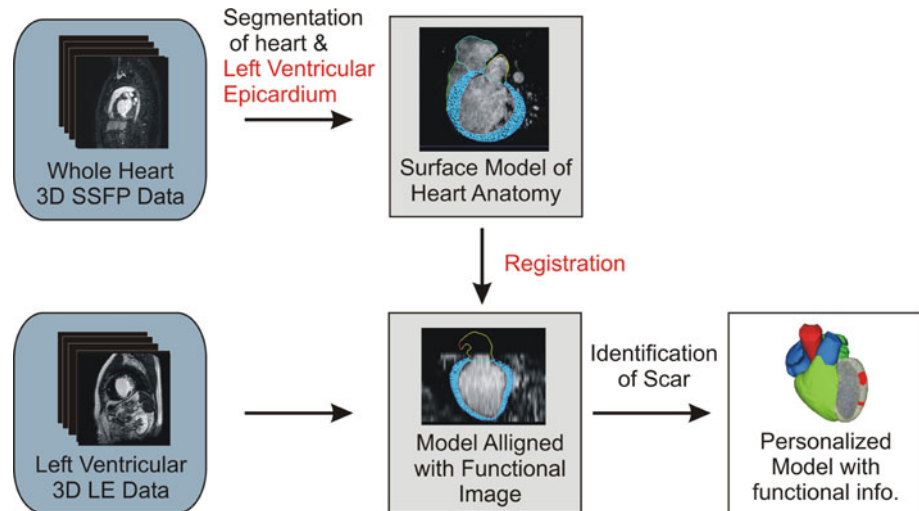
steady-state free-precession (SSFP) MR scans. The volumetric mesh also included in the reference model is reconstructed afterwards between the patient-specific LV epi- and endocardium by minimization of a shape preserving internal energy. Then, the personalized anatomical model is registered to late enhancement (LE) MR scans showing the scar distribution. This step is also realized by the model-based segmentation framework. In particular, model adaptation with features trained on the LE MR images is performed, while no shape deformations are allowed and shape transformations are restricted to a global rigid transformation. By thresholding, it is decided for each tetrahedron of the volumetric mesh if it covers scar or healthy tissue.

The resulting accuracy of the viability information depends to a large extent on the accuracy of both the anatomical model and the mapping of the model to the LE image. For the considered 3D SSFP MR images, the LV endocardium can be segmented robustly, but the epicardium is often hardly visible. To improve the segmentation, the epicardium is linked to the shape of the endocardium (cf. also [28]). To reflect the observed variability of inter-patient myocardium thickness, the myocardium thickness is corrected by a patient-specific factor measured at a reliable location like the interventricular septum. Thereby it is assumed that this deviation from the model is similar in all regions of a patient's LV myocardium which might not hold under specific disease conditions. Using 20 clinical 3D SSFP MR data sets, it was shown that the proposed shape-bias for the epicardium reduces the segmentation error of the LV epicardium from 1.28 to 1.17 mm [24].

2.2 Vessel segmentation

Apart from shape of the whole heart including the four chambers also the supplying and draining vessels are

Fig. 2 Processing pipeline for integrating ventricular scar information from LE scans into a heart model derived from an anatomical image (color figure online)



essential for a comprehensive heart model. For example, for simulating the electrophysiology in CRT it is desirable to complement the anatomical heart model with the coronary venous system assuming a placement of LV lead through the coronary venous tree [13].

Well-known vessel segmentation techniques [34] are intensity-based methods [48], generalized cylinder approximations [56], multiscale [45, 52] and skeletonization [58] schemes, and deformable model approaches [25, 36] applied on successive 2D slices or on volume data. In our approach, a geometrical moment-based tracking algorithm is applied to magnetic resonance angiography (MRA) datasets to extract the coronary venous system. Initially, the algorithm was designed for the lower limb vessel extraction [54] and coronary arteries [10] in multislice CT angiography (MSCTA). Its principle is based on the assumption that a vessel can be locally approximated by a cylinder. Then, analytical expressions of 3D geometrical moments of up to order two are used in association with local intensity information to compute the local orientation of the cylinder axis and its diameter. The initialization of the tracking is performed from a list of seed points, interactively selected at a preliminary stage. From one seed point P_i , its position is first refined through an iterative process to make it converge towards the central axis. Then the local diameter is estimated using a multiscale local moment computation to take into account the size variation of the vessel. Afterwards, the tracking process is carried out by shifting a circular window towards a point $P_i + 1$ according to the estimated direction at point P_i . The incremental displacement between these two points is made adaptive and depends on the vessel size and curvature.

This algorithm has been revised to enforce its robustness in weak contrast and noisy data sets. These improvements focused on the centreline extraction and included:

1. The regularization of the tracking direction with the application of an infinite impulse response (IIR) filtering on the successive directions;
2. The search for the optimal location of the centreline through the construction of a set of paths, based on a multiple hypothesis testing procedure [55];
3. The selection of the optimal path for each coronary vein branch by means of a graph-based method: it consisted of the still-leaf of the graph, in applying a minimum spanning tree algorithm [20] followed by graph erosion [38].

Once the vein centerlines have been extracted, the vessel lumen was extracted from the local radius estimation at each central axis position. The latter one was computed using the cylinder equation, the background and vessel mean intensity computed inside and outside the vessel, and the zero order geometric moment.

Extractions have been carried out on four MRA volumes from different patients, acquired with the same SSFP MR

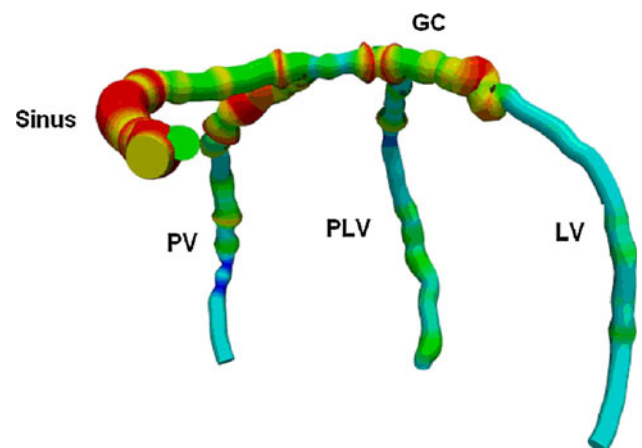
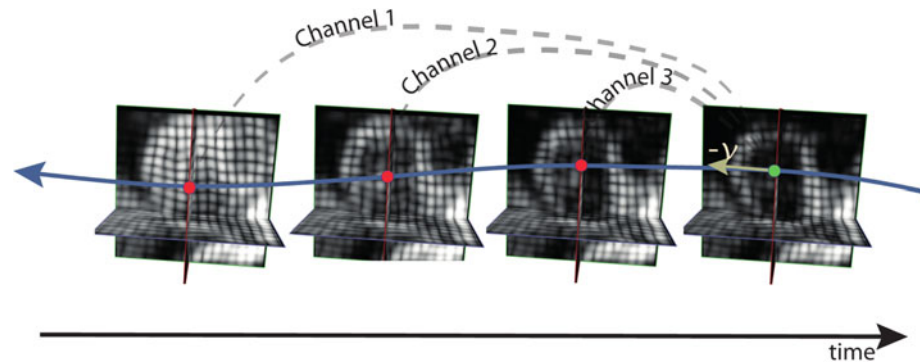


Fig. 3 Coronary vein extraction (diameters in color) (color figure online)

Fig. 4 Illustration of the coupling in the TDFFD algorithm where several image pairs of the sequence (*channels*) contribute to the optimization of the velocity at one time point



sequence. Image resolutions are 0.58×0.58 mm in the image planes, and interslice distances range from 0.75 to 0.9 mm. Figure 3 displays the result including the coronary sinus (Sinus), the great cardiac vein (GC), the posterior vein (PV) and postero-lateral vein (PLV), and the lateral vein (LV).

2.3 Motion analysis

The quantification of cardiac motion and strain provides insight into cardiac function through the assessment of how a given pathology affects global and local deformation of the myocardium. For instance, the measurement of the relative timing of regional myocardial tissue motion helps to identify the type of dyssynchrony of each CRT candidate and the selection criteria for therapy [17]. Hence, personalized physiological simulations with comprehensive physiological heart models should be enriched by heart motion analysis.

Applying non-rigid registration for quantifying cardiac deformation has been thoroughly investigated both in tagged MR [57] and 3D ultrasound images [2, 21]. However, most of these approaches align images in a sequential manner, without exploiting the natural redundancy in the images sequence. Spatiotemporal registration methods solve for the full motion field, taking the whole image sequence as input [32, 37, 41]. In parallel, diffeomorphic registration techniques [7] substituted the classical representation of a non-rigid transformation using displacement fields by velocity fields. Diffeomorphic registration was first extended to temporal image sequences by [29].

Our temporal diffeomorphic free form deformation (TDFFD) algorithm [14] replaces the representation of the dense velocity field used in [29] by a B-spline representation continuous in space and time. Starting from a point in a reference frame (green point in Fig. 4), the point can be transported to other frames by following the flow of the velocity field and the interpolated intensities (red points in Fig. 4) can be matched to the intensity of the reference frame. Every pair of frames in the sequence can be seen as one observation channel to optimize the velocity field. Indeed, as suggested in Fig. 4, a variation of velocity in

one frame modifies the interpolated intensities in all “channels”. Thus, when computing the metric gradient in the space of velocity parameters, e.g., for a specific time, derivative contributions from adjacent frames are transported to this time. This transport involves the parametric derivative of the velocity field at the transported time points and the volume change introduced by the transformation between the two considered instants.

The simultaneous use of multiple channels during motion estimation in combination with the B-spline representation of the velocity field that is continuous in space and time is expected to improve the robustness of the motion quantification algorithm. Indeed, it was shown in [14] that the TDFFD algorithm was more accurate at low levels of signal to noise ratios in synthetic ultrasound images with known ground truth motion compared to a classical pairwise approach.

The algorithm was originally designed for 3D ultrasound images, where artifacts specific to this modality make motion and deformation quantification a challenging problem [14]. The algorithm was then applied on tagged MR images [15, 53], extending the original metric with a fixed reference to incorporate sequential frame intensity differences. Temporal continuity of the TDFFD algorithm was exploited in [44] to compensate for temporal and spatial misalignments when quantifying motion and deformation from several 3D ultrasound image sequences.

Figure 5 shows an example of the recovered longitudinal strain curves from 3D ultrasound images from a healthy subject at mid and basal AHA segments. Uniform strain patterns were observed over all myocardial segments as physiologically expected.

3 Integration of image analysis and biophysical simulations

3.1 Encoding of structures for simulations

Personalized physiological simulations of the heart [50] often require knowledge about microstructures. This

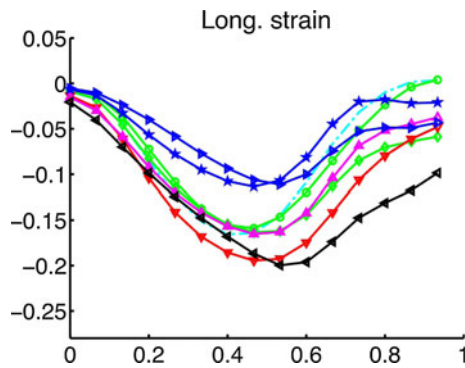


Fig. 5 Longitudinal strain for a healthy volunteer visualized as temporal curve per AHA (American Heart Association) segment. Only segments that were totally included in the field of view of the 3D ultrasound image sequence are shown. The *horizontal axis* is the normalized cardiac time (from 0 to 1)

includes, for example, the atrial fast conduction tracts or muscle fiber directions [16]. Because such structures are hardly visible in clinical images, a direct, individualized segmentation is not feasible to date. However, these structures are visible in histological studies [26] or specialized measurements, such that their typical location can be defined in a simulation model.

To avoid intermediate processing steps like atlas mapping [43], we use a generic interface to directly attach microstructures to the heart models used for model-based segmentation [40]. Since the mesh resolution in model-based segmentation is optimized for segmentation, it is generally too low to simply attach microstructures to mesh vertices. To overcome this limitation, we encoded the microstructures *relative to* the segmentation mesh into the model prior to adaptation (Fig. 6). After adapting the model to the image [19], the mesh elements have been deformed and the relative coordinates of a structure with respect to a mesh element are used to reconstruct a specific location.

In particular, a segmentation mesh is composed of a set of vertices forming surface triangles or volumetric tetrahedra. A location on or in the mesh can be described by the

index of the respective mesh element and by a vector of local coordinates. Points defined in that way can be used to define specific structures such as the sinus node, crista terminalis, pectinate muscles, Bachmann’s bundle or the inferior isthmus. Muscle fiber directions can be represented, as well. Figure 7 shows two examples.

The approach assumes that the encoded structures show little anatomical variability between different individuals. In addition, the approach assumes that vertex positions of the generic model are mapped to corresponding anatomical positions in the adaptation process. To investigate to what extent the latter assumption is satisfied, $N = 37$ CT scans acquired at the same heart phase (diastasis/reduced filling) with very good segmentation quality were used and model-based segmentation has been performed with varying shape of the reference model. The resulting vertex displacements on the model surface has been measured after model adaptation leading to an average overall accuracy of 1.6 mm for corresponding vertex positions.

The error of encoded structures has been determined by averaging the errors in the respective area on the model surface. The average positional deviation along the surface of the left ventricle was around 1.5 mm allowing to encode muscle fiber directions without much loss of precision. For sinus node, crista terminalis, pectinate muscles, Bachmann’s bundle, and right atrial inferior isthmus in the atria, the error was below 2 mm.

3.2 Aorta segmentation with pressure constraint

Various approaches exist with respect to vessel segmentation [34]. Most approaches for aorta segmentation have been developed for 3D CT or MR images, but also aorta segmentation in 3D + T image time-series has been considered [9, 60]. Segmentation of the aorta is of special interest in the context of arterial hemodynamics. However, patient-specific calculation of blood flow through the aorta as a function of time requires the simultaneous mechanical modeling of the vessel walls as well as flow within the lumen of the vessel. Especially, the dimensions and patient-specific material

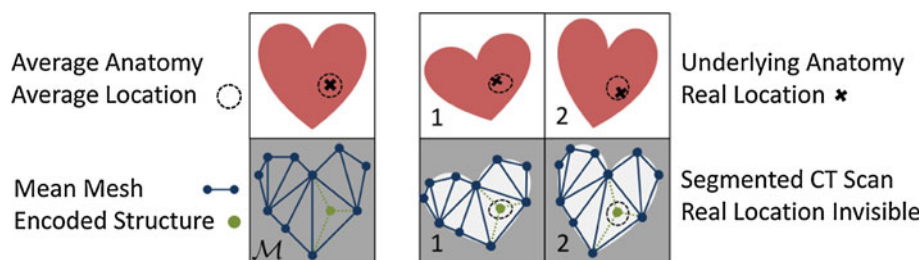
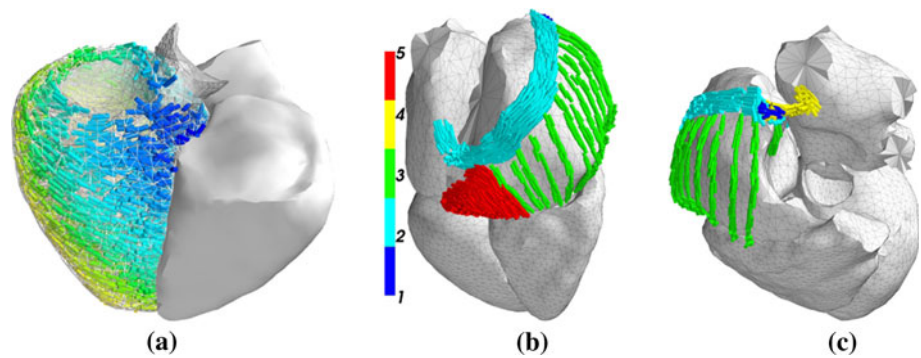


Fig. 6 Interface for structure encoding. Functional structures (*green*) are encoded by linear combinations (*thin dotted lines*) of vertices of the segmentation mesh (*blue*) elements such as triangles or tetrahedra

(*left*). The mesh can be adapted to patient anatomies and the encoded structures transform accordingly (*right*) (color figure online)

Fig. 7 Examples for structure encoding. **a** Ventricular muscle fiber directions. **b, c** Atrial fast conduction pathways, where the colors correspond to 1 sinus node, 2 crista terminalis, 3 pectinate muscles, 4 Bachmann's bundle, and 5 inferior isthmus (color figure online)



properties of the wall are required, but these physiological constraints are difficult to obtain. This section outlines how information about the material properties of the wall, as a function of distance along the vessel, can be extracted from 4D images of the aorta. The material properties can then be used in the fluid structure interaction (FSI) computation.

Arterial hemodynamics and especially the blood pressure and flow-velocity wave forms have been studied for a long time [3]. For an idealized cylindrical axi-symmetric vessel with linear wall material, the pressure in the vessel as a function of distance along the vessel and time obeys the 1D wave equation. The pressure difference with respect to a reference point is proportional to the associated fractional radius change (FRC). The proportionality factor can be either related to Young's modulus describing tissue stiffness or to the pressure wave velocity. Measuring the FRC can therefore supply information about the variation of these properties along the vessel.

Gated CT or MRI can be used to generate a time sequence of 3D images. A mean or reference image can be derived from these images. Each of the images in the 3D sequence is mapped to the reference image using image registration [4, 5]. The reference image is segmented to generate a binary image (reference segment) of the lumen and this segment is then mapped back to each individual image using the previously computed mappings. A further mapping is generated, which maps the reference segment to a cylinder, and this mapping is applied to each of the segments in the sequence (Fig. 8a).

To determine the FRC between the image slice of the reference segment and the image slice of another segment at a distinct time point, an optical flow approach as in [5] restricted to a radial transform and simple translation can be used. The optical flow approach leads to one equation for every pixel, and the resulting set of simultaneous equations can be robustly solved for the unknown FRC and translation.

The equations for all slice pairs can be aggregated together in matrix vector form and solved simultaneously. However, even if aggregated the values of the FRC as function of distance along the vessel and time are

determined independently of the others. The computed values are therefore inevitably corrupted by noise in the image data. Since for the ideal cylinder the FRC obeys the wave equation, this fact can be imposed as a Tikhonov regularization on the solution of the set of simultaneous equations. To this end, a constraint is derived from the form of the wave equation [6], ensuring that the resulting values of the FRC (Fig. 8b) satisfy both the data and the constraint.

If the dimensions and material properties do not change along the vessel there is a simple scaling relationship between pressure and FRC. In reality, this will not be the case. Vessels change in radius along their length and material properties may change. Generally, in the latter portion of the cardiac cycle the aortic flow is close to zero. During this phase, the pressure along the aorta is uniform (although it will generally decrease over time). This observation can be used to scale the FRC data to a surrogate of pressure (Fig. 9). Finally, if a diastolic and systolic pressure measurement at some point along the aorta is available, the surrogate curve can be scaled to obtain absolute values of material properties (or wave-speed) along the aorta (Fig. 10).

Aorta segmentation with pressure constraint requires an estimate of wave-speed. Initially, the registration can be performed using literature values (normal ranges are 5–10 m/s) to obtain a first approximation of the wave speed curve. In a second iteration, an updated version of the wave speed curve is obtained using the data from the first run.

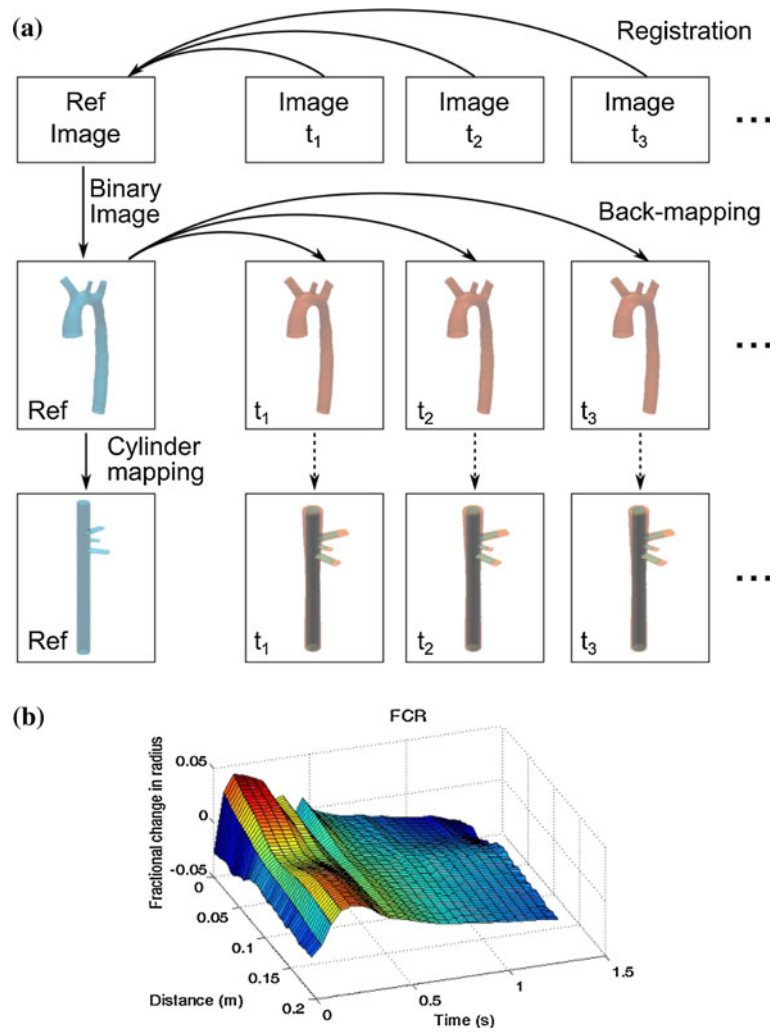
This algorithm has been validated using idealized cylindrical data, with and without a radius changing along the vessel, and using an FSI simulation on a patient's anatomy.

4 Examples

4.1 Comprehensive model for a CRT case

We illustrate generation of a comprehensive heart model with the methods described in the previous sections using a

Fig. 8 **a** Flow diagram for segmenting the aorta in time series of images. **b** Exemplary fractional changes r in radius



patient case for CRT treatment acquired at St. Thomas’ Hospital, London, UK. To this aim, three different MR data sets were acquired. From steady-state free-precession (SSFP) scans, the anatomical model and the coronary veins are segmented. Late enhancement (LE) scans are used to extract the myocardial scar in the left ventricle. The generic muscle fiber directions have been encoded into the anatomical reference model and reconstructed after model adaptation. From a sequence of tagged MR images, the motion of the left ventricle is determined including the calculation of strain. Figure 11 shows the resulting model.

4.2 Simulation of anisotropic excitation propagation

In order to demonstrate our pipeline from image to simulation, first electrophysiological simulations in the atria were performed. For that purpose, we encoded additional information into the segmentation mesh: first, the simulation mesh itself, which has a four times higher resolution than the segmentation mesh. Second, we encoded the

location of the crista terminalis and its fiber direction (see Fig. 7). We circumvented intermediate registration steps (cf. [31] as an example for the mesh creation for simulating large deformation mechanics from patient-specific anatomy) by our direct encoding approach. Excitation propagation was simulated by the anisotropic eikonal equation for wave propagation, which we solved by a fast marching algorithm [47]. In Fig. 12, we compare an isotropic and an anisotropic simulation as done in [30]. We used the double velocity along the fibers and half the velocity orthogonal to the fibers in the anisotropic case. One can clearly see that the shape of the wavefront distinctively differs (as in [30]). This shows that structure encoding is required for personalizing electrophysiological simulations.

5 Discussion and conclusion

Heart chamber segmentation, vessel segmentation and deformation estimation algorithms have been developed in

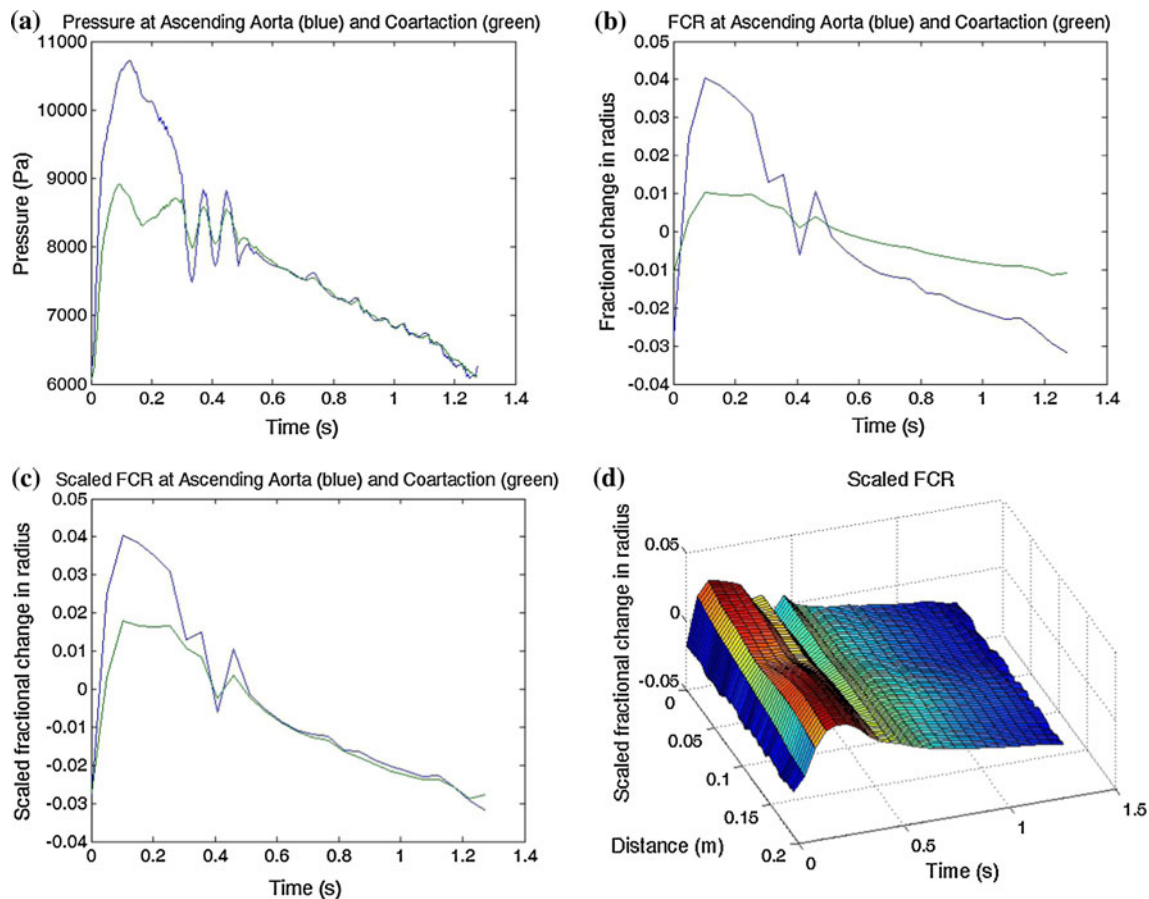


Fig. 9 **a** Pressure in the ascending aorta (*blue*) and the coarctation (*green*). **b** Fractional changes in radius at the ascending aorta (*blue*) and the coarctation (*green*). **c** Scaled fractional changes in radius at

the ascending aorta (*blue*) and the coarctation (*green*). **d** Scaled fractional radius changes (color figure online)

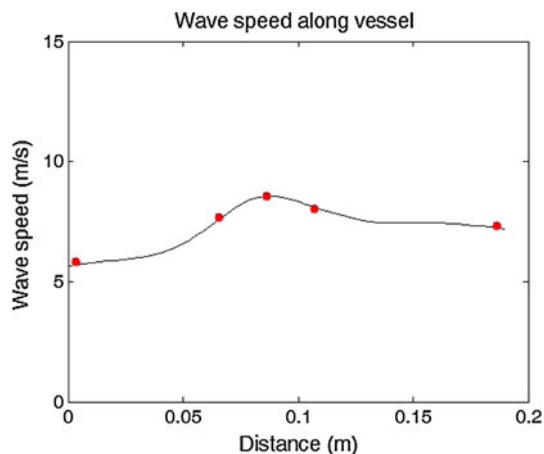


Fig. 10 Wavespeed along the vessel. The *red points* represent wavespeed calculated at points where pressure measurements were available (ascending and descending aorta, mid coarctation, and two further points). The *solid line* is the relative wave speed scaled using the *red points* to obtain the real wave speed over the whole vessel (color figure online)

the European integrated project euHeart. Particular attention was paid to needs that are relevant for physiological simulations such as the integration of scar tissue information in

the context of CRT. In addition, two approaches to closely link image processing and simulations have been presented. The first one allows to encode structures and information for simulations into segmentation meshes and to efficiently set up simulations. The second one directly integrates biophysical constraints with image analysis.

The direct integration of biophysical constraints with image analysis looks promising. The example of aorta segmentation from time-series of images using a pressure constraint shows the potential to assess tissue properties and improve data interpretation. This approach seems to be an alternative to simulation-based methods for the characterization of tissue properties, where simulation parameters are adapted to match medical images or other bio-signals. Such a parameter adaptation approach was used in [8] to estimate the artery wall stiffness in an idealized abdominal aortic aneurysm and in [11] to determine tissue stiffness and contractility in the left ventricular myocardium from tagged MR.

Physiological simulations rely often on a sophisticated and complex processing pipeline. Application in a clinical

Fig. 11 Heart model with coronary veins of a CRT patient. **a** Scar information of the LV myocardium is *color-coded* into the muscle fiber direction *arrows* (blue no scar, red scar, intermediate colors due to interpolation). **b** Anatomical model with scar and **c** with *color-coded* circumferential strain (color figure online)

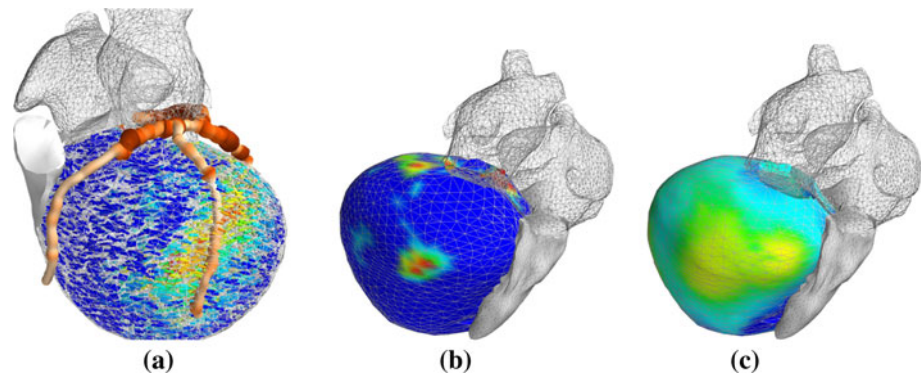
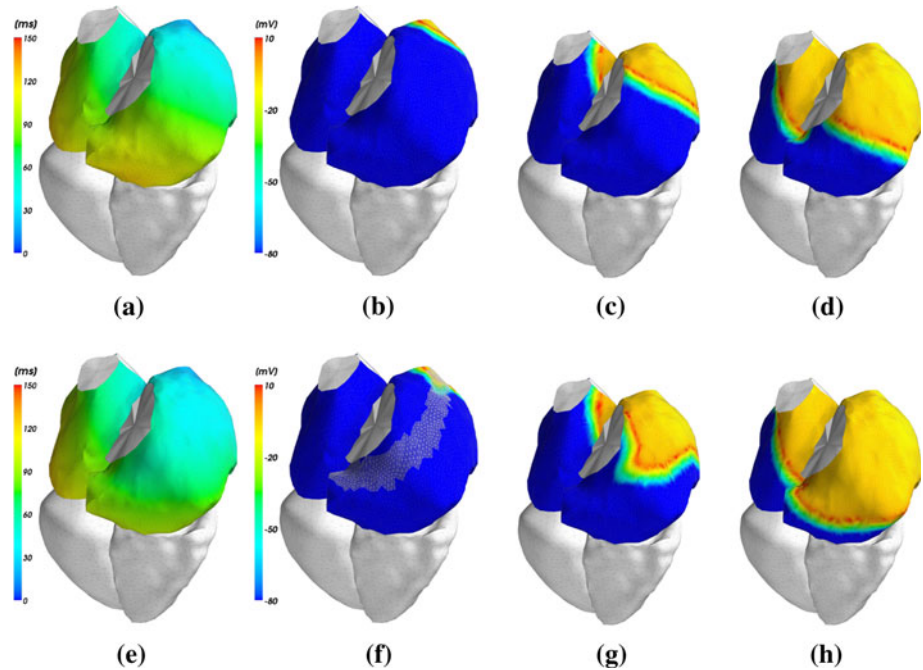


Fig. 12 Excitation propagation in the human atria. Isotropic (**a–d**) and anisotropic (**e–h**) propagation using the crista terminalis. Local activation times (*left*), and transmembrane voltages after 30, 60, and 90 ms (*right*)



context requires, however, efficient and largely automated processing pipelines. Encoding of structures and information for simulations into segmentation meshes may help to simplify and automate processing pipelines as has been illustrated in the example of excitation propagation in the left atrium. Linking of this mechanism to evolving standards like the FieldML (field modelling/mark-up language) description [12] may be considered in the future.

Both approaches for closely linking image processing and simulations show directions of how physiological simulations provide new stimuli and challenges for future image analysis research. The use of biophysical or physiological constraints in image analysis has the potential to improve data interpretation in many cases. Efficient approaches for patient-specific model building are essential to pave the way of virtual physiological simulations for clinical use on a large number of cases.

Acknowledgments The research leading to these results has received funding from the European Community's Seventh

Framework Programme (FP7/2007-2013) under grant agreement number 224495 (euHeart project).

References

1. Aguado-Sierra J, Krishnamurthy A, Villongco C, Chuang J, Howard E, Gonzales M, Omens J, Krummen D, Narayan S, Kerckhoffs R et al (2011) Patient-specific modeling of dyssynchronous heart failure: a case study. *Prog Biophys Mol Biol* 107(1):147–155
2. Angelini E, Gerard O (2006) Review of myocardial motion estimation methods from optical flow tracking on ultrasound data. *Engineering in medicine and biology society*, pp 1537–1540
3. Avolio A, Westerhof BE, Siebes M, Tyberg JV (2009) Arterial hemodynamics and wave analysis in the frequency and time domains: an evaluation of the paradigms. *Med Biol Eng Comput* 47(2):107–110
4. Barber DC, Hose DR (2005) Automatic segmentation of medical images using image registration diagnostic and simulation applications. *J Med Eng Technol* 29(2):53–63
5. Barber DC, Oubel E, Frangi AF, Hose DR (2007) Efficient computational fluid dynamics mesh generation by image registration. *Med Image Anal* 11(6):648–662

6. Barber DC, Shi Y, Staicu C, Berrbaum P, Valverde I, Baginska J, Rutten MCM, Gaddum N, Hose DR (2011) Measurement of aortic pressure wave velocity by 4D image registration. In: Medical image understanding and analysis
7. Beg M, Miller M, Trounev A, Younes L (2005) Computing large deformation metric mappings via geodesic flows of diffeomorphisms. *Int J Comput Vis* 61(2):139–157
8. Bertoglio C, Moireau P, Gerbeau J (2012) Sequential parameter estimation for fluid–structure problems: application to hemodynamics. *Int J Numer Methods Biomed Eng* 28(4):434–455
9. Biesdorf A, Wörz S, Müller T, Weber TF, Heye T, Hosch W, von Tengg-Koblighk H, Rohr K (2011) Model-based segmentation and motion analysis of the thoracic aorta from 4D ECG-gated CTA images. *Lecture Notes in Computer Science (MICCAI)* 6891: 589–596
10. Bousse A, Boldak C, Toumoulin C, Yang G, Laguitton S, Boulmier D (2006) Coronary extraction and characterization in multi-detector computed tomography. *ITBM-RBM* 27(5-6): 217–226
11. Chabiniok R, Moireau P, Lesault PF, Rahmouni A, Deux JF, Chapelle D (2001) Trials on tissue contractility estimation from cardiac cine MRI using a biomechanical heart model. *Lecture Notes in Computer Science (FIMH)* 6666:304–312
12. Christie GR, Nielsen PM, Blackett SA, Bradley CP, Hunter PJ (2009) FieldML: concepts and implementation. *Philos Trans R Soc A* 367(1895):1869–1884
13. Daubert J, Ritter P, Le Breton H, Gras D, Leclercq CAL, Mugica J, Mabo P, Cazeau S (1998) Permanent left ventricular pacing with transvenous leads inserted into the coronary veins. *PACE* 21:239–245
14. De Craene M, Piella G, Camara O, Duchateau N, Silva E, Doltra A, D’hooge J, Brugada J, Sitges M, Frangi AF (2012) Temporal diffeomorphic free-form deformation: application to motion and strain estimation from 3d echocardiography. *Med Image Anal* 16(2):427–450
15. De Craene M, Tobón-Gomez C, Butakoff C, Duchateau N, Piella G, Rhode KS, Frangi AF (2011) Temporal diffeomorphic free form deformation (TDFFD) applied to motion and deformation quantification of tagged mri sequences. *Lecture Notes in Computer Science (STACOM)* 7085:68–77
16. Dössel O, Krueger MW, Weber FM, Wilhelms M, Seemann G (2012) Computational modeling of the human atrial anatomy and electrophysiology. *Med Biol Eng Comput* 50(8):773–799
17. Duchateau N, De Craene M, Piella G, Silva E, Doltra A, Sitges M, Bijneens B, Frangi A (2011) A spatiotemporal statistical atlas of motion for the quantification of abnormal myocardial tissue velocities. *Med Image Anal* 15(3):316–328
18. Ecabert O, Peters J, Schramm H, Lorenz C, von Berg J, Walker MJ, Vembar M, Olszewski ME, Subramanyan K, Lavi G, Weese J (2008) Automatic model-based segmentation of the heart in CT images. *IEEE Trans Med Imag* 27(9):1189–1201
19. Ecabert O, Peters J, Walker MJ, Ivanc T, Lorenz C, von Berg J, Lessick J, Vembar M, Weese J (2011) Segmentation of the heart and great vessels in CT images using a model-based adaptation framework. *Med Image Anal* 15(6):863–876
20. Eisner J (1997) State-of-the-art algorithms for minimum spanning trees: a tutorial discussion. University of Pennsylvania
21. Elen A, Choi H, Loeckx D, Gao H, Claus P, Suetens P, Maes F, D’hooge J (2008) Three-dimensional cardiac strain estimation using spatio-temporal elastic registration of ultrasound images: a feasibility study. *IEEE Trans Med Imag* 27(11):1580–1591
22. euHeart consortium: <http://www.euheart.eu/>
23. Ferrant M, Nabavi A, Macq B, Jolesz FA, Kikinis R, Warfield SK (2001) Registration of 3-D intraoperative MR images of the brain using a finite-element biomechanical model. *IEEE Trans Med Imag* 20(12):1384–1397
24. Groth A, Weese J, Lehmann H (2012) Robust left ventricular myocardium segmentation for multi-protocol MR. *SPIE Med Imaging* 8314:83142S1–83142S9
25. Hernández Hoyos M, Orkisz M, Roux J, Douek P (1999) Inertia-based vessel axis extraction and stenosis quantification in 3D MRA images. In: *Computer assisted radiology and surgery (CARS)*, pp 189–193
26. Ho SY, Sanchez-Quintana D (2008) The importance of atrial structure and fibers. *Clin Anat* 22:52–63
27. Joldes GR, Wittek A, Warfield SK, Miller K (2012) Performing brain image warping using the deformation field predicted by a biomechanical model. *Comput Biomech Med* 1:89–96
28. Kaus MR, von Berg J, Weese J, Niessen W, Pekar V (2004) Automated segmentation of the left ventricle in cardiac MRI. *Med Image Anal* 8(3):245–254
29. Khan A, Beg M (2008) Representation of time-varying shapes in the large deformation diffeomorphic framework. In: *Biomedical imaging: from nano to macro (ISBI)*, pp 1521–1524
30. Krueger MW, Schmidt V, Tobón C, Weber FM, Lorenz C, Keller DUJ, Barschdorf H, Burdumy M, Neher P, Plank G, Rhode KS, Seemann G, Sánchez-Quintana D, Saiz J, Razavi R, Dössel O (2011) Modeling atrial fiber orientation in patient-specific geometries: a semi-automatic rule-based approach. *Lecture Notes in Computer Science (FIMH)* 6666:223–232
31. Lamata P, Niederer S, Nordsletten D, Barber DC, Roy I, Hose DR, Smith N (2011) An accurate, fast and robust method to generate patient-specific cubic Hermite meshes. *Med Image Anal* 15(6):801–813
32. Ledesma-Carbayo M, Kybic J, Desco M, Santos A, Suhling M, Hunziker P, Unser M (2005) Spatio-temporal nonrigid registration for ultrasound cardiac motion estimation. *IEEE Trans Med Imag* 24(9):1113–1126
33. Lehmann H, Kneser R, Neizel M, Peters J, Ecabert O, Kühl H, Kelm M, Weese J (2008) Integrating viability information into a cardiac model for interventional guidance. *Lecture Notes in Computer Science (FIMH)* 5528:312–320
34. Lesage D, Angelini ED, Bloch I, Funka-Lea G (2009) A review of 3D vessel lumen segmentation techniques: models, features and extraction schemes. *Med Image Anal* 13(6):819–845
35. Lorenz C, Berg J (2006) A comprehensive shape model of the heart. *Med Image Anal* 10(4):657–670
36. Lorigo LM, Faugeras OD, Grimson WEL, Keriven R, Kikinis R, Nabavi A, Westin CF (2001) Curves: curve evolution for vessel segmentation. *Med Image Anal* 5:195–206
37. Metz C, Klein S, Schaap M, Van Walsum T, Niessen W (2011) Nonrigid registration of dynamic medical imaging data using n-d+t b-splines and a groupwise optimization approach. *Med Image Anal* 15(2):238–249
38. Nacken P, Toet A, Vincent L (1992) Graph morphology. *J Vis Commun Image Represent* 3(1):24–38
39. Neher P, Barschdorf H, Dries S, Weber FM, Krueger MW, Dössel O, Lorenz C (2011) Automatic segmentation of cardiac CTs—personalized atrial models augmented with electrophysiological structures. *Lecture Notes in Computer Science (FIMH)* 6666:80–87
40. Nickisch H, Barschdorf H, Weber FM, Krueger MW, Dössel O, Weese J (2012) From image to personalized cardiac simulation: encoding anatomical structures into a model-based segmentation framework. *Lecture Notes in Computer Science (STACOM)* (accepted)
41. Oubel E, De Craene M, Hero AO, Pourmorteza A, Huguet M, Avegliano G, Bijneens BH, Frangi AF (2012) Cardiac motion estimation by joint alignment of tagged mri sequences. *Med Image Anal* 16(1):339–350
42. Peters J, Ecabert O, Meyer C, Schramm H, Kneser R, Groth A, Weese J (2007) Automatic whole heart segmentation in static

- magnetic resonance image volumes. *Lecture Notes in Computer Science (MICCAI)* 4792:402–410
43. Peyrat JM, Sermesant M, Pennec X, Delingette H, Xu C, McVeigh ER, Ayache N (2007) A computational framework for the statistical analysis of cardiac diffusion tensors: application to a small database of canine hearts. *IEEE Trans Med Imag* 26(10):1–15
 44. Piella G, De Craene M, Yao C, Penney GP, Frangi AF (2011) Multiview diffeomorphic registration for motion and strain estimation from 3D ultrasound sequences. *Lecture Notes in Computer Science (FIMH)* 6666:375–383
 45. Sato Y, Nakajima S, Shiraga N, Atsumi H, Yoshida S, Koller T, Gerig G, Kikinis R (1998) Three-dimensional multi-scale line filter for segmentation and visualization of curvilinear structures in medical images. *Med Image Anal* 2(2):143–168
 46. Sermesant M, Chabiniok R, Chinchapatnam P, Mansi T, Billet F, Moireau P, Peyrat JM, Wong K, Relan J, Rhode K, Ginks M, Lambiase P, Delingette H, Sorine M, Rinaldi CA, Chapelle D, Razavi R, Ayache N (2012) Patient-specific electromechanical models of the heart for the prediction of pacing acute effects in CRT: a preliminary clinical validation. *Med Image Anal* 16(1):201–215
 47. Sermesant M, Konukoğlu E, Delingette H, Coudière Y, Chinchapatnam P, Rhode KS, Razavi R, Ayache N (2007) An anisotropic multi-front fast marching method for real-time simulation of cardiac electrophysiology. *Lecture Notes in Computer Science (FIMH)* 4466:160–169
 48. Shiffman S, Rubin G, Napel S (2000) Medical image segmentation using analysis of isolable-contour maps. *IEEE Trans Med Imag* 19(11):1064–1074
 49. Sigg DC, Iaizzo PA, Xiao Y-F, He B (2010) *Cardiac electrophysiology methods and models*. Springer, London
 50. Smith N, de Vecchi A, McCormick M, Nordsletten D, Camara O, Frangi AF, Delingette H, Sermesant M, Relan J, Ayache N, Krueger MW, Schulze WHW, Hose R, Valverde I, Beerbaum P, Staicu C, Siebes M, Spaan J, Hunter P, Weese J, Lehmann H, Chapelle D, Razavi R (2011) euHeart: personalized and integrated cardiac care using patient-specific cardiovascular modelling. *Interface Focus* 1(3):349–364
 51. Streeter D, Spontnitz H, Patel D, Ross J, Sonnenblick E (1969) Fiber orientation in the canine left ventricle during diastole and systole. *Circ Res* 24:339–347
 52. Summers P, Bhalerao A, Hawkes D (1997) Multiresolution, model-based segmentation of mr angiograms. *J Magn Reson Imaging* 7(6):950–957
 53. Tobón-Gomez C, De Craene M (2011) A multimodal database for the 1st cardiac motion analysis challenge. *Lecture Notes in Computer Science (STACOM)* 7085:33–44
 54. Toumoulin C, Boldak C, Dillenseger JL, Coatrieux JL, Rolland Y (2001) Fast detection and characterization of vessels in very large 3-D data sets using geometrical moments. *IEEE Trans Biomed Eng* 48(5):604–606
 55. Velut J, Toumoulin C, Coatrieux JL (2010) 3D coronary structure tracking algorithm with regularization and multiple hypotheses in MRI. In: *Biomedical imaging: from nano to macro (ISBI)*, pp 37–40. Piscataway, NJ, USA
 56. Verdonck B, Bloch L, Maitre H, Vandermeulen D, Suetens P, Marchal G (1996) Accurate segmentation of blood vessels from 3D medical images. In: *International conference on image processing (ICIP)* 3:311–314
 57. Wang H, Amini A (2012) Cardiac motion and deformation recovery from MRI: a review. *IEEE Trans Med Imag* 31(2):487–503
 58. Wilson DL, Noble JA (1997) Segmentation of cerebral vessels and aneurysms from mr angiography data. In: *Information processing in medical imaging (IPMI)*, pp 423–428
 59. Wittek A, Miller K, Kikinis R, Warfield SK (2007) Patient-specific model of brain deformation: application to medical image registration. *J Biomech* 40(4):919–929
 60. Zhao F, Zhang H, Wahle A, Thomas MT, Stolpen AH, Scholz TD, Sonka M (2009) Congenital aortic disease: 4D magnetic resonance segmentation and quantitative analysis. *Med Image Anal* 13(3):483–493
 61. Zheng Y, Barbu A, Georgescu B, Scheuering M, Comaniciu D (2008) Four-chamber heart modeling and automatic segmentation for 3D cardiac CT volumes using marginal space learning and steerable features. *IEEE Trans Med Imag* 27(11):1668–1681